Automatic Extraction of Transport Model Parameters of an Organic Semiconductor Material

Pasquale Claudio Africa, Dario A. Natali, Mario Caironi, and Carlo de Falco

Abstract In Africa et al. (Sci Rep 7(1):3803, 2017) a step-by-step procedure was presented that enables to determine the density of states width, the carrier mobility and the injection barrier height of an OTFT structure by fitting data from simple measurements to suitable numerical simulations. At each step of the procedure only one parameter value is determined, thus highly simplifying the fitting procedure and enhancing its robustness. In this study we apply such procedure to p-type organic polymers. A very satisfactory fitting of experimental measurements is obtained, and physically meaningful values for the aforementioned parameters are extracted thus further confirming the soundness of the parameter extraction method.

1 Introduction

The relatively easy and inexpensive processing techniques for organic semiconductors (e.g., they can be deposited by means of printing techniques adapted from graphical arts (ink-jet, screen printing, spray coating, flexography to cite but a few [1]) make them suitable candidates for the development of large-area, low cost, flexible electronics [2]). Their electronic performance has been constantly improving leading to devices which some times even outperform those based on amorphous silicon [3]. Many fundamental physical questions, though,

P. C. Africa · C. de Falco (✉)
MOX Modelling and Scientific Computing, Dipartimento di Matematica, Politecnico di Milano, Milano, Italy
e-mail: pasqualeclaudio.africa@polimi.it; carlo.defalco@polimi.it

D. A. Natali
Dipartimento di Elettronica, Informazione, Bioingegneria, Politecnico di Milano, Milano, Italy

Center for Nano Science and Technology @PoliMi, Istituto Italiano di Tecnologia, Milano, Italy
e-mail: dario.natali@polimi.it

M. Caironi
Center for Nano Science and Technology @PoliMi, Istituto Italiano di Tecnologia, Milano, Italy
e-mail: francesco.maddalena@iit.it; mario.caironi@iit.it

G. Nicosia, V. Romano (eds.), *Scientific Computing in Electrical Engineering*, Mathematics in Industry 32, https://doi.org/10.1007/978-3-030-44101-2_9

are still debated and there is a strong need for simple yet reliable approaches for extracting physical parameters from experimental measurements [4]. In [5] it was shown that, by fitting Capacitance-Voltage (CV) measurements of Metal-Insulator-Semiconductor (MIS) capacitors, it is possible to extract the width of the Density of States (DOS) exploiting the sensitivity of CV curves to the degree of disorder. Performing measurements on MIS capacitors at low frequency, quasi-equilibrium is ensured so that simulations can be performed in the static regime and phenomena specifically related to carrier transport are negligible for fitting experimental measurements; as a result the DOS extraction is disentangled from carrier transport properties, which makes the fitting procedure substantially simpler and more robust. If the DOS is assumed to be Gaussian, the carrier mobility can be predicted in the framework of the Extended Gaussian Disorder Model (EGDM)[6], and used to successfully fit the transfer characteristic curves of OTFTs in the linear regime. The DOS width extraction requires the accurate knowledge of the device geometrical dimensions, of the insulator and semiconductor permittivities, of the total density of available states and of the metal/semiconductor injection barrier (Φ_B) between the bottom metal and the semiconductor. This latter parameter is the one that is affected by highest level of uncertainty. Actually, metal/semiconductor interfaces are still a subject of debate in the scientific community [7]; due to the various phenomena which may be involved the prediction of Φ_B is a hard task, and its measurement requires expensive dedicated equipment. The uncertainty in Φ_B results in an uncertainty in the extracted value of the DOS width, as shown in [8]: for each given value of Φ_B a different value for the DOS width results from fitting. As reported in Sect. 5, the uncertainty is not negligible indeed: by varying Φ_B from 2 eV down to 0.25 eV, the DOS width reduces from about 9 k_BT down to about 2 k_BT. In [5] it was demonstrated that this uncertainty can be drastically reduced by cooperatively exploiting MIS CV curves, MIS Capacitance-Frequency (CF) curves and OTFT transfer characteristic curves in the linear regime. To this end, as discussed in [8] the simulation domain needs to cover out-of-equilibrium conditions in the framework of the Drift-Diffusion (DD) model. This allows to simulate the whole CF curve of the MIS capacitor. In addition, in the modeling and fitting of OTFT transfer characteristic curves the contact resistance needs to be accounted for in the context of the current crowding regime [9, 10].

In [8] the simultaneous extraction procedure was successfully applied to Poly{[N,N′-bis(2-octyldodecyl)-naphthalene-1,4,5,8-bis(dicarboximide)-2,6-diyl]-alt-5,5′-(2,2′-bithiophene)} (P(NDI2OD-T2)), a printable, prototypical n-type polymer. Here we adapt the model to p-type materials then we assess its accuracy when applied to Poly(2,5-bis(3-tetradecylthiophen-2-yl)thieno[3,2-b]thiophene) (PBTTT) based devices.

To model charge transport in transient regime, we employ the Drift-Diffusion model, which is described in Sect. 2 [11–13]. Transient simulations are used to compute the voltage and frequency dependence of the small-signal capacitance of the MIS capacitor. The most notable feature of the DD model described in this contribution are: (1) the charge injection boundary condition at the metal/semiconductor

interface, and (2) the dependence of the mobility and of the diffusion coefficient on the DOS width.

While useful for computing the capacitance over a wide range of frequencies, the full DD model turns out to be of too high complexity and of insufficient numerical accuracy for efficiently fitting measured low-frequency CV curves. For this reason a modified version of the Non-linear Poisson (NLP) model is derived in Sect. 3, which includes a more accurate description of the contact injection barrier with respect to previous work [5], and is therefore fully consistent with the zero-frequency limit of the complete DD model.

The latter extended NLP model naturally describes the effect of the deviation from Einstein's relation but, as it is derived for the quasi-static regime, it does not require to model the mobility coefficient.

The models used for computing the transfer characteristics of the OTFT device are object of discussion in Sect. 4.

2 The Transient Drift-Diffusion Model

The setting for numerically simulating the MIS, shown in Fig. 1, consists of a one-dimensional schematization of the device along normal direction z to the semiconductor/insulator interface [5]. Denote by Ω_{sc}, Ω_{ins} the semiconductor and insulator regions respectively (such that $\Omega = \Omega_{sc} \cup \Omega_{ins}$ is the whole computational domain) and by T the simulated timespan.

The DD model consists of the following system of partial differential equations

$$-\frac{\partial}{\partial z}\left(\varepsilon \frac{\partial \varphi}{\partial z}\right) - \rho = 0 \quad \text{in } \Omega \times T, \tag{1}$$

$$\frac{\partial p}{\partial t} + \frac{1}{\mathrm{q}} \frac{\partial J_p}{\partial z} = 0, \quad \text{in } \Omega_{sc} \times T, \tag{2}$$

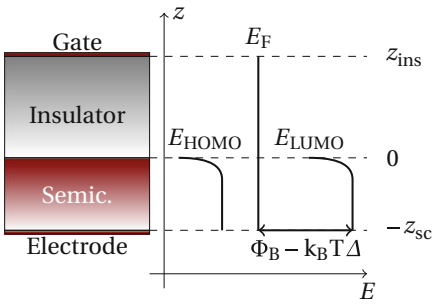

Fig. 1 One-dimensional schematic of the MIS capacitor used for the analysis and related energy levels

for the electrostatic potential φ and the hole density p, where ε is the electrical permittivity, ρ the charge density, q is the quantum of charge and J_p the hole current density. Neglecting trapped charges and dopant ion density, $\rho = +\mathrm{q}p$ in Ω_{sc} while, $\rho = 0$ in insulating regions.

The current density consists of drift and diffusion contributions

$$J_p = -\mathrm{q}\left(D_p \frac{\partial p}{\partial z} + \mu_p p \frac{\partial \varphi}{\partial z}\right), \tag{3}$$

D_p and μ_p denoting the diffusion and mobility coefficients respectively.

In the following we will assume a Gaussian shape for the DOS[5, 14–16] which may be expressed as

$$P(E, E_{\mathrm{HOMO}}) = \frac{N_0}{\sqrt{2\pi\sigma^2}} \exp\left[-\frac{(E - E_{\mathrm{HOMO}})^2}{2\sigma^2}\right], \tag{4}$$

where N_0 denotes the total density of hopping sites, E_{HOMO} the Highest Occupied Molecular Orbital (HOMO) energy level and σ the DOS width. Having assumed the ansatz (4) for the DOS, it is possible to express the mobility coefficient according to the EGDM [17]

$$\mu_p = \mu_{0,p}\, g_1(p)\, g_2(\mathcal{E}), \tag{5}$$

where $\mu_{0,p}$ is the low-field and low-density mobility and the two enhancement factors g_1 and g_2 account respectively for the dependence on the carrier density p and on the electric field $\mathcal{E}$. The analytical expression for the enhancement factors is given in [5, 8, 17].

Charge injection/extraction at the metal/semiconductor interface is modeled by imposing that carrier density at the contact relaxes with finite velocity v_p to an equilibrium value p_0 which depends on the intensity and direction of the normal electric field at the contact

$$J_p = \mathrm{q}\, v_p \cdot (p - p_0)\,.$$

Following [18] we adopt models for v_n and n_0 that result in a variant of the well known injection model developed by Scott and Malliaras[11, 19]. Further details on the boundary conditions imposed on the DD system are collected in Sect. 2.2.

2.1 The Modified Einstein Relation

The diffusion and mobility coefficients D_p and μ_p in (3) are related via the generalized Einstein relation[17]:

$$D_p = g_3(p(E_{\mathrm{HOMO}}, E_{\mathrm{F}}))\, \frac{\mathrm{k_B T}}{\mathrm{q}}\, \mu_p.$$

Assuming Fermi–Dirac statistics for the occupation probability of electron energy states, the electron density may be expressed as

$$p(E_{\mathrm{HOMO}}, E_{\mathrm{F}}) = \int_{-\infty}^{+\infty} P(E, E_{\mathrm{HOMO}}) \left[1 - \frac{1}{1 + \exp\left(\frac{E - E_{\mathrm{F}}}{\mathrm{k_B T}}\right)} \right] \mathrm{d}E, \tag{6}$$

where E_{F} denotes the Fermi level, $\mathrm{k_B}$ the Boltzmann constant and T the temperature, and the dimensionless diffusion enhancement factor g_3 is given by

$$g_3(p) = \left(\mathrm{k_B T} \frac{\partial p}{\partial E_{\mathrm{F}}} \right)^{-1} p.$$

The partial derivative $\partial p / \partial E_{\mathrm{F}}$ can be computed by substituting Eq. (4) into (6) and by applying a suitable change of the integration variable, yielding

$$p(E_{\mathrm{HOMO}}, E_{\mathrm{F}}) = \frac{N_0}{\sqrt{\pi}} \int_{-\infty}^{+\infty} e^{-\eta^2} \left[1 + \exp\left(\frac{\sqrt{2}\sigma\eta - E_{\mathrm{HOMO}} + E_{\mathrm{F}}}{\mathrm{k_B T}} \right) \right]^{-1} \mathrm{d}\eta.$$

2.2 Boundary Conditions for the Drift-Diffusion Equations

Let z_{sc} and z_{ins} be the thickness of the semiconductor and insulator layer respectively (so that $\Omega_{sc} = \{z : -z_{\mathrm{sc}} \leq z \leq 0\}$ and $\Omega_{ins} = \{z : 0 < z \leq z_{\mathrm{ins}}\}$). The values of the electric potential at the ends of the computational domain are given by

$$\begin{aligned} \varphi|_{z=-z_{\mathrm{sc}}} &= -\Phi_B/\mathrm{q} \\ \varphi|_{z=z_{\mathrm{ins}}} &= V_{\mathrm{g}} + V_{\mathrm{shift}}, \end{aligned}$$

where Φ_B is the zero-field value of the Schottky barrier height and V_{shift} is a model parameter accounting for effects such as permanent dipoles, fixed charge in dielectrics or metal work function mismatch [5]. At the metal/semiconductor interface charge injection/extraction is represented by the following Robin boundary condition

$$J_p\big|_{z=-z_{\mathrm{sc}}} = \mathrm{q}\, v_p \cdot \left(p|_{z=-z_{\mathrm{sc}}} - p_0 \right), \tag{7}$$

where p_0 is the equilibrium charge density, expressed as

$$p_0 = \frac{N_0}{\sqrt{\pi}} \int_{-\infty}^{+\infty} e^{-\eta^2} \left[1 + \exp\left(\frac{\sqrt{2}\sigma\eta + \Phi_B}{\mathrm{k_B T}} - \Delta \right) \right]^{-1} \mathrm{d}\eta.$$

Following the description in [11], the coefficient Δ accounts for Schottky barrier lowering/increase depending on the field at the electrode

$$\Delta = \begin{cases} \sqrt{f}, & \text{if } f \geq 0 \text{ (carrier injection)}, \\ f/4, & \text{if } f < 0 \text{ (carrier extraction)}, \end{cases}$$

where $f = \mathrm{q}\mathcal{E}r_\mathrm{c}/(\mathrm{k_B T})$ is the reduced inward electric field and $r_\mathrm{c} = \mathrm{q}^2/(4\pi\varepsilon_\mathrm{sc}\mathrm{k_B T})$ the Coulomb radius. The recombination velocity v_p in the injection regime is given by

$$v_p(f) = \frac{4\pi\varepsilon(\mathrm{k_B T})^2\mu_{0,p}}{\mathrm{q}^3}\left(\frac{1}{\psi^2(f)} - f\right), \qquad \psi(f) = f^{-1} + f^{-\frac{1}{2}} - f^{-1}\left(1 + 2f^{\frac{1}{2}}\right)^{\frac{1}{2}},$$

while, in the carrier extraction regime ($f < 0$), $v_p(f) = v_p(0)$. Finally, at the semiconductor/insulator interface

$$J_p\big|_{z=0} = 0. \tag{8}$$

3 The Stationary Non-linear Poisson Model

The DD equations presented above completely describe the devices under study and could in principle be used in any operation regime (stationary, transient, AC, ...). Unfortunately, given the strict tolerances and the large number of simulation runs required by the parameter fitting algorithm described in [5], the DD model may lead to unaffordable computational costs. Fortunately in the simulation of CV curves in the static regime, the model complexity can be significantly reduced. Indeed, in the stationary regime, Eq. (8) implies that $J_n = 0$ everywhere and that the carrier density does not depend on time. As a result the Fermi potential E_F is constant in both space and time (and may be set to 0 without loss of generality). System (1)–(2) reduces to the following NLP equation

$$-\frac{\partial}{\partial z}\left(\varepsilon\frac{\partial\varphi}{\partial z}\right) - \mathrm{q}\,p(\varphi) = 0, \qquad \text{in } \Omega$$

$$p(\varphi) = \frac{N_0}{\sqrt{\pi}}\int_{-\infty}^{+\infty} e^{-\eta^2}\left[1 + \exp\left(\frac{\sqrt{2}\sigma\eta + \mathrm{q}\varphi}{\mathrm{k_B T}} - \Delta\right)\right]^{-1} \mathrm{d}\eta,$$

$$\varphi|_{z=-z_\mathrm{sc}} = -\Phi_B/\mathrm{q},$$

$$\varphi|_{z=-z_\mathrm{sc}} = V_\mathrm{g} + V_\mathrm{shift}.$$

This model extends the NLP equation presented in [5] in order to account for the Schottky barrier lowering due to charge injection phenomena. We also remark

that the boundary condition at the metal/semiconductor interface is consistent with Eq. (7), i.e. $p|_{z=-z_{sc}} = p_0$. The procedure for accurately deducing the device low-frequency capacitance from charge and potential profiles is described in Ref.[5, 20].

4 OTFT Currents in the Linear Operation Regime

Once the DOS width σ has been extracted by fitting static CV curves, the low-field, low-density mobility $\mu_{0,p}$ can be determined by computing OTFT transfer characteristics in the linear regime. The drain-to-source current is expressed as $I_{DS}(V_g) = V_{DS}/R_{tot}(V_g)$, where V_{DS} is the potential drop across the channel and $R_{tot} = R_{ch} + R_C$ is the total device resistance, accounting for both the channel and the contact resistance contributions. The channel resistance R_{ch} is given by:

$$R_{ch} = \left[\frac{W}{L}\int_{-z_{sc}}^{0} q\mu_p(z)p(z)dz\right]^{-1}, \tag{9}$$

W and L being the channel width and length respectively. As in [8–10], R_C accounts for current crowding effects and is obtained considering contributions due to the resistance met by the current flow: (1) across the semiconductor thickness, from the source contact to the accumulated channel (R_y); and (2) along the accumulated channel (R_{sh}) in the overlap region between the source contact and the gate contact. It is modeled as $R_C = R_y/[WL_0\tanh(L_{ov}/L_0)]$, where L_{ov} is the overlap length between the gate and the source/drain electrodes, $L_0 = \sqrt{R_y/R_{sh}}$ and

$$R_{sh} = \left[\int_{-z_{sc}}^{0} q\mu_p(z)p(z)dz\right]^{-1}, \tag{10}$$

$$R_y = \int_{-z_{sc}}^{0} \left[q\mu_p(z)p(z)\right]^{-1} dz. \tag{11}$$

The integrand functions in Eqs. (9)–(11) are computed by simulating, as highlighted in Fig. 2, two different one-dimensional cross-sections along the z direction corresponding to the middle of the channel (R_{ch}, R_{sh}) and to the source contact (R_y) respectively. The mobility coefficient $\mu_p(z)$ is expressed through the EGDM model (5), where $\mathcal{E} = V_{DS}/L$ is the drain-to-source field. The total current I_{DS} is known up to the multiplicative constant $\mu_{0,p}$, which is then extracted by fitting numerical and experimental Current–Voltage (IV) curves through a least-squares procedure. The fitting residual can finally be exploited to determine the best fitting value of Φ_B, as shown in Fig. 5.

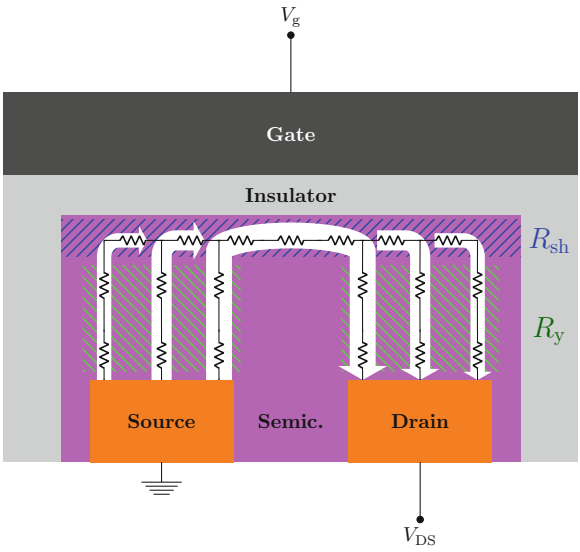

Fig. 2 Sketch of the OTFT under current crowding effects

5 Results and Discussion

The parameter estimation procedure described in [8] was applied to the extraction of physical model parameters of the p-type PBTTT semiconductor, starting from experimental data on a MIS capacitor and an OTFT based on this polymer.

Experimental data taken from [5] would lead to estimate a nominal injection barrier $\Phi_B = 0.9$ eV. As described in [8], the uncertainty in determining a physically meaningful value of Φ_B affects other physical properties as obtained by fitting the MIS experimental CV curve, which leads to the dependence of σ and the contact resistance R_C on Φ_B shown in Figs. 3 and 4 respectively.

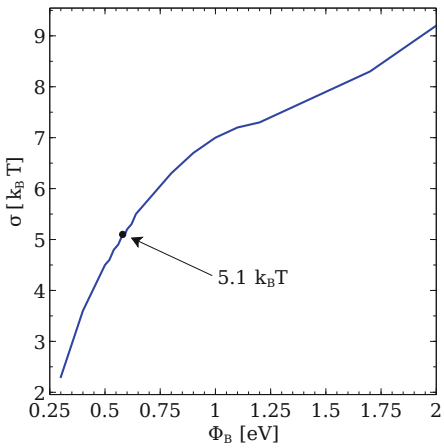

Fig. 3 Dependence of the fitted Gaussian DOS width σ on the injection barrier Φ_B. The dot on the curve identifies the σ value that simultaneously yields in the best fitting of OTFT transfer characteristic curves and of MIS capacitor CF curves

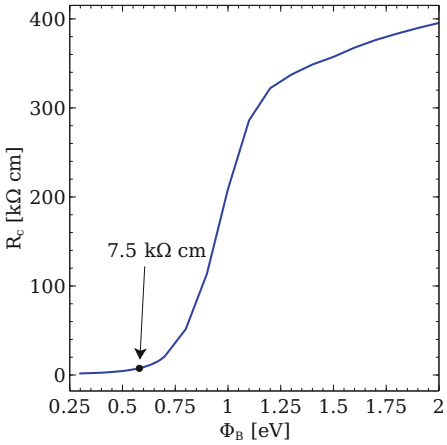

Fig. 4 Contact resistance R_C (at $V_{gate} = +35$ V) for different values of the injection barrier Φ_B. The dots on the curves identify the Φ_B value that simultaneously yields in the best fitting of OTFT transfer characteristic curves and of MIS capacitor CF curves

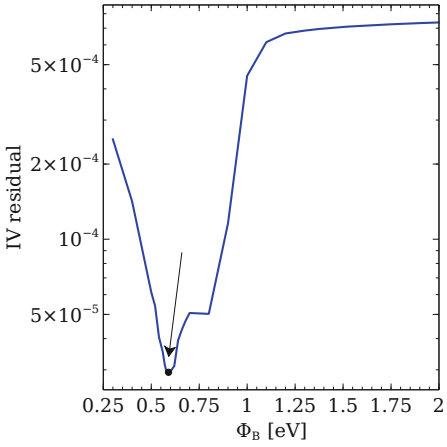

Fig. 5 Residual of the least-squares fit of the OTFT transfer characteristic curves with contact resistance effects taken into account, at different values of the injection barrier Φ_B

However, the uncertainty can be reduced by fitting IV transfer characteristics of the OTFT. The procedure yields to the residual in Fig. 5 that has a unique minimum, corresponding to the optimal barrier value $\Phi_B = 0.58$ eV and, accordingly, $\sigma = 5.1\ k_BT$ and $\mu_{0,p} = 7.84 \cdot 10^{-8}\ cm^2\ V^{-1}\ s^{-1}$. The resulting fitted CV and IV curves, compared to experimental data, are shown in Figs. 6 and 7, respectively.

In this case experimental CF curves are limited to a narrow range of frequencies. Therefore, the validation of the values extracted is not as clear as in the case of P(NDI2OD-T2) since both the nominal and the optimal set of parameters seem to provide a good agreement to experimental measurements, as reported in Fig. 8.

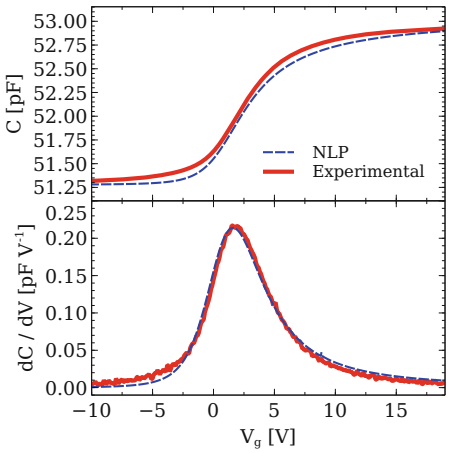

Fig. 6 CV curve and derivative, computed for the optimal barrier $\Phi_B = 0.58$ eV. Experimental CV shown for comparison

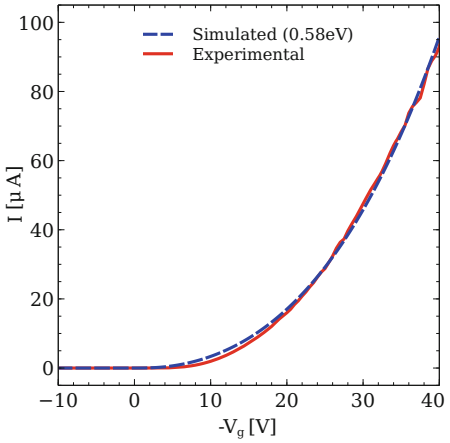

Fig. 7 Comparison between experimental (red) and simulated OTFT transcharacteristics at the optimal barrier value $\Phi_B = 0.58$ eV

Anyhow, the ratio between the capacitance computed in the accumulation and in the depletion regime shows that the nominal barrier leads to a capacitance drop at a low frequency of about 10^3 Hz that is not seen in experimental data, while the optimal barrier results in a plateau extending to a range that perfectly matches the one seen in experiments.

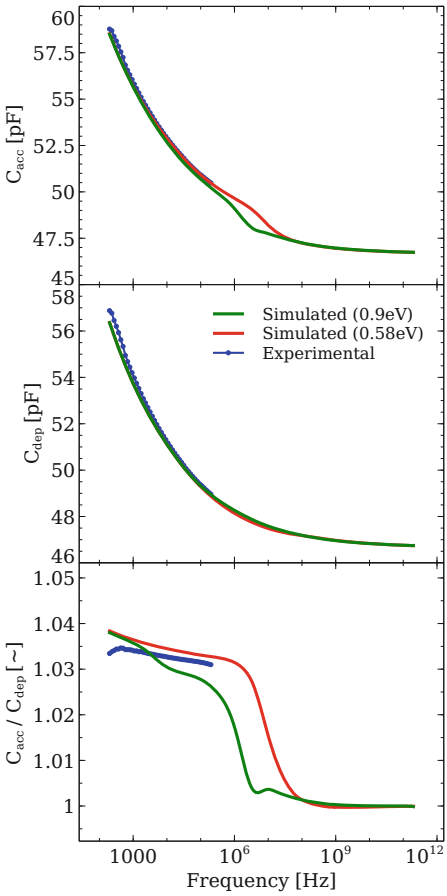

Fig. 8 CF curves in the accumulation regime ($V_{gate} = +35$ V), the depletion regime ($V_{gate} = -15$ V) and normalized, computed for the nominal injection barrier $\Phi_B = 0.9$ eV and for the optimal barrier $\Phi_B = 0.58$ eV. Experimental CF characteristics shown for comparison

References

1. Katsuaki, S.: Introduction to Printed Electronics. Springer, New York (2014)
2. Caironi, M., Noh, Y.Y.: Large Area and Flexible Electronics. Wiley–VCH, Weinheim (2015)
3. Paterson, A.F., Singh, S., Fallon, K.J., Hodsden, T., Han, Y., Schroeder, B.C., Bronstein, H., Heeney, M., McCulloch, I., Anthopoulos, T.D.: Recent progress in high-mobility organic transistors: a reality check. Adv. Mater. **30**(36) (2018)
4. de Vries, R.J., Badinski, A., Janssen, R.A.J., Coehoorn, R.: Extraction of the materials parameters that determine the mobility in disordered organic semiconductors from the current-voltage characteristics: accuracy and limitations. J. Appl. Phys. **113**(11), 114505 (2013)
5. Maddalena, F., de Falco, C., Caironi, M., Natali, D.: Assessing the width of Gaussian density of states in organic semiconductors. Org. Electron. **17**, 304–318 (2015)
6. Coehoorn, R., Pasveer, W.F., Bobbert, P.A., Michels, M.A.J.: Charge-carrier concentration dependence of the hopping mobility in organic materials with Gaussian disorder. Phys. Rev. B **72**(15), 155206 (2005)
7. Oehzelt, M., Koch, N., Heimel, G.: Organic semiconductor density of states controls the energy level alignment at electrode interfaces. Nat. Commun. **5**, 4174 (2014)

8. Africa, P.C., de Falco, C., Maddalena, F., Caironi, M., Natali, D.: Simultaneous extraction of density of states width, carrier mobility and injection barriers in organic semiconductors. Sci. Rep. **7**(1), 3803 (2017)
9. Natali, D., Caironi, M.: Charge injection in solution-processed organic field-effect transistors: physics, models and characterization methods. Adv. Mater. **24**(11), 1357–1387 (2012)
10. Jung, K.D., Kim, Y.C., Kim, B.J., Park, B.G., Shin, H., Lee, J.D.: An analytic current-voltage equation for top-contact organic thin film transistors including the effects of variable series resistance. Jpn. J. Appl. Phys. **47**(4S), 3174 (2008)
11. Barker, J.A., Ramsdale, C.M., Greenham, N.C.: Modeling the current-voltage characteristics of bilayer polymer photovoltaic devices. Phys. Rev. B **67**(7), 075205 (2003)
12. de Falco, C., Sacco, R., Verri, M.: Analytical and numerical study of photocurrent transients in organic polymer solar cells. Comput. Methods Appl. Mech. Eng. **199**(25–28), 1722–1732 (2010)
13. de Falco, C., Porro, M., Sacco, R., Verri, M.: Multiscale modeling and simulation of organic solar cells. Comput. Methods Appl. Mech. Eng. **245–246**, 102–116 (2012)
14. Coehoorn, R., Bobbert, P.A.: Effects of Gaussian disorder on charge carrier transport and recombination in organic semiconductors. Phys. Status Solidi A **209**(12), 2354–2377 (2012)
15. Bässler, H., Köhler, A.: Charge transport in organic semiconductors. Top. Curr. Chem. **312**, 1–65 (2012)
16. Baranovskii, S.D.: Theoretical description of charge transport in disordered organic semiconductors. Phys. Status Solidi B **251**(3), 487–525 (2014)
17. van Mensfoort, S., Coehoorn, R.: Effect of Gaussian disorder on the voltage dependence of the current density in sandwich-type devices based on organic semiconductors. Phys. Rev. B **78**(8), 085207 (2008)
18. Santoni, F., Gagliardi, A., der Maur, M.A., Di Carlo, A.: The relevance of correct injection model to simulate electrical properties of organic semiconductors. Org. Electron. **15**(7), 1557–1570 (2014)
19. Scott, J.C., Malliaras, G.G.: Charge injection and recombination at the metal-organic interface. Chem. Phys. Lett. **299**(2), 115–119 (1999)
20. de Falco, C., O'Riordan, E.: Interior layers in a reaction-diffusion equation with a discontinuous diffusion coefficient. Int. J. Numer. Anal. Model. **7**(4), 444–461 (2010)